NANO LETTERS

pubs.acs.org/NanoLett

Letter

Compact Super Electron-Donor to Monolayer MoS_2

Serrae N. Reed-Lingenfelter, Yifeng Chen, Milad Yarali, David J. Charboneau, Julia B. Curley, David J. Hynek, Mengjing Wang, Natalie L. Williams, Nilay Hazari, Su Ying Quek, and Judy J. Cha*

Cite This: *Nano Lett.* 2022, 22, 4501−4508

Read Online

ACCESS | Metrics & More | Article Recommendations | Supporting Information

ABSTRACT: The surface functionalization of two-dimensional (2D) materials with organic electron donors (OEDs) is a powerful tool to modulate the electronic properties of the material. Here we report a novel molecular dopant, Me-OED, that demonstrates record-breaking molecular doping to MoS_2, achieving a carrier density of 1.10 ± 0.37 × 10^{14} cm^{-2} at optimal functionalization conditions; the achieved carrier density is much higher than those by other OEDs such as benzyl viologen and an OED based on 4,4′-bipyridine. This impressive doping power is attributed to the compact size of Me-OED, which leads to high surface coverage on MoS_2. To confirm, we study ^{t}Bu-OED, which has an identical reduction potential to Me-OED but is significantly larger. Using field-effect transistor measurements and spectroscopic characterization, we estimate the doping powers of Me- and ^{t}Bu-OED are 0.22−0.44 and 0.11 electrons per molecule, respectively, in good agreement with calculations. Our results demonstrate that the small size of Me-OED is critical to maximizing the surface coverage and molecular interactions with MoS_2, enabling us to achieve unprecedented doping of MoS_2.

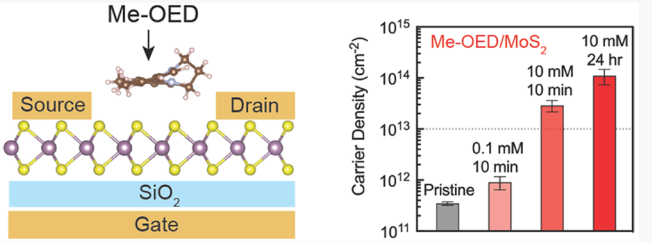

KEYWORDS: *Two-dimensional materials, molybdenum disulfide, surface functionalization, molecular doping, atomic force microscopy (AFM), electric transport properties*

Surface functionalization of two-dimensional (2D) materials with organic molecules is a powerful tool to modulate the properties of 2D materials, in part due to our ability to synthesize molecular dopants with tailored structures and functionalities.[1] Since the seminal study of graphene functionalized with organic electron donors (OEDs) in 2007, the optical, electronic, and magnetic properties of a number of 2D materials have been modified using surface functionalization.[2−23] Noteworthy results include the reversible doping of MoS_2 using benzyl viologen[8] and the high carrier density of 5.8 ± 1.9 × 10^{13} cm^{-2} achieved in MoS_2 via surface functionalization with an organic dopant based on 2,2′-bipyridine (DMAP-OED).[4] Generally, the amount of charge doping from OEDs is predicted based on the relative position of the molecule's redox potential in relation to the Fermi level of the 2D host.[6,24] However, other factors, such as the steric properties of the molecule, the nature of the interaction between the molecule and the 2D material, and interactions between the molecules on the 2D material, also impact the overall charge donation but are not as well understood.[4,17,25,26] On the basis of these preliminary studies, we hypothesize that optimization of both the redox and steric properties of a molecular dopant is essential for the design of powerful dopants.

Here we report a novel molecular dopant, Me-OED, which demonstrates record molecular doping to MoS_2, achieving a carrier density of 1.10 ± 0.37 × 10^{14} cm^{-2} at optimal functionalization conditions. We attribute the high doping power of Me-OED to its compact size (surface area of ∼65 $Å^2$ per molecule), which leads to high coverage of the MoS_2 surface. To confirm, we study as a control ^{t}Bu-OED, which has the same redox potential as Me-OED but a larger surface area (∼90 $Å^2$ per molecule). We quantify the doping powers of the two OEDs by (i) measuring the change in carrier density of MoS_2 field-effect transistors (FETs) before and after functionalization, and (ii) estimating the number of molecules that functionalize MoS_2 using atomic force microscopy (AFM). At optimal functionalization conditions, we show that the doping powers of Me- and ^{t}Bu-OED are 0.22−0.44 and 0.11 electrons per molecule, respectively. Thus, despite having identical redox potentials, the two OEDs donate different amounts of electrons to MoS_2 due to differences in size, which affects their interaction with MoS_2. Density functional theory (DFT) calculations are performed for the two OEDs at different surface coverages and assist in understanding the experimental results. Further, Me-OED also outperforms DMAP-OED, our previous record-holding molecular dopant to MoS_2, which has a significantly more

Received: March 30, 2022
Revised: May 20, 2022
Published: May 24, 2022

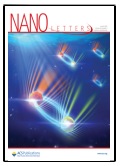

https://doi.org/10.1021/acs.nanolett.2c01167
Nano Lett. 2022, 22, 4501−4508

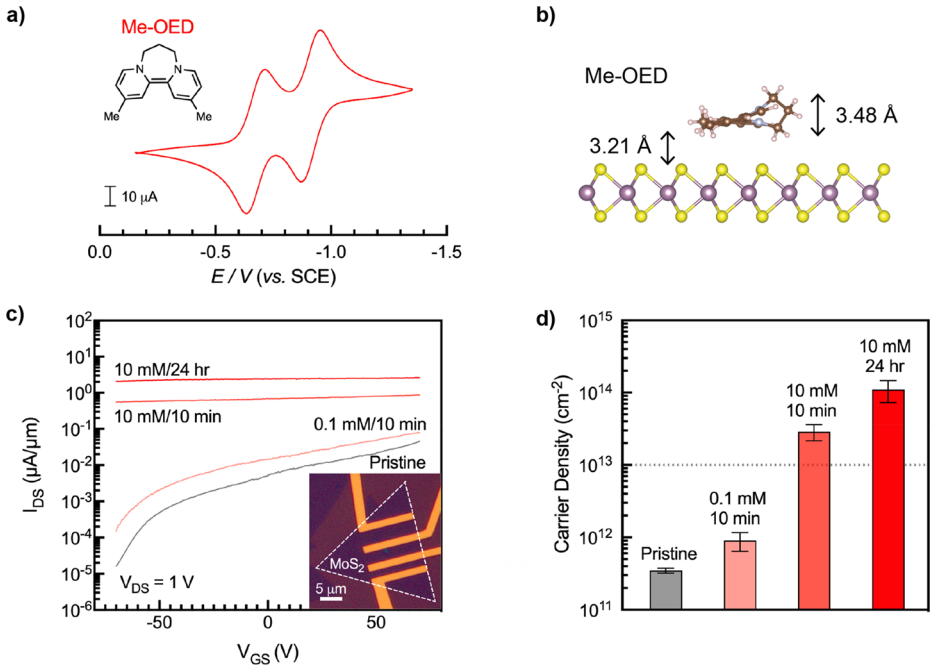

Figure 1. Cyclic voltammogram (CV) of Me-OED and transfer characteristics of MoS_2 transistors. (a) Chemical structure and CV scan of Me-OED, indicating the redox potentials of −0.91 V and −0.67 V versus SCE. (b) Atomic structure of a Me-OED molecule on MoS_2 from DFT calculations. (c) I_{DS}−V_{GS} transfer curves of MoS_2 FETs functionalized with Me-OED at three different functionalization conditions: 10 mM/24 h (top), 10 mM/10 min (middle), and 0.1 mM/10 min (bottom), with a pristine MoS_2 FET in gray for comparison. The bias voltage is 1 V and the channel length of the devices is 3 μm. Inset: Optical image of a pristine MoS_2 FET with varying channel lengths. (d) Systematic increase of the average carrier density of MoS_2 functionalized with Me-OED at V_{GS} = 0 V with increasing solution concentration and functionalization time. The error bars represent the standard error obtained from measuring 4 to 6 MoS_2 devices.

negative redox potential but a larger surface area than Me-OED.[4] Overall, our results establish that the steric properties of OEDs critically affect their doping power and are a crucial factor to consider, alongside redox potential, in the design of new OEDs.

Me-OED is a novel neutral reductant that is stable and soluble in organic solvents under an inert atmosphere (Supporting Information Section S1). Figure 1a shows the cyclic voltammogram and molecular structure of Me-OED. It undergoes two discrete one-electron transfer events at −0.91 V and −0.67 V versus the saturated calomel electrode (SCE). Accordingly, electron transfer is expected from the Me-OED molecule to MoS_2.[8] Figure 1b shows the ground state structure of a Me-OED molecule on monolayer MoS_2, as determined using DFT calculations (Supporting Information Section S1). The aromatic rings of an isolated Me-OED molecule are nearly parallel to the basal plane of MoS_2.

Back-gated MoS_2 FETs were fabricated on monolayer MoS_2 flakes via chemical vapor deposition, and their electrical properties were measured before and after functionalization in ambient atmosphere (Figure S1; Supporting Information Section S1). Me-OED solutions were prepared and drop-cast on MoS_2 FETs in an argon-filled glovebox. After being exposed for the desired functionalization time, the FETs were washed with acetonitrile. We systematically varied the functionalization conditions (solution concentration and functionalization time) and measured the transfer characteristics of the pristine and functionalized devices (Figure 1c, which is shown in linear scale in Figure S2). At a bias voltage of 1 V, the pristine MoS_2 FET shows strong gate dependency with expected n-type transport. We note that the extracted two-contact field-effect mobility values for pristine samples are low (>1 $cm^2/(V\ s)$), which we attribute to environmental effects from measuring the devices in ambient as well as potential high contact resistance at the MoS_2/electrode interface. After functionalization with 0.1 mM and 10 mM Me-OED solutions for 10 min, the drain current (I_{DS}) at zero gate voltage (V_{GS}) increased by one and two orders of magnitude, respectively. The gate dependency of the current is significantly diminished for the devices functionalized with 10 mM Me-OED solution, indicating that Me-OED is a potent n-type dopant.[8] We observe that a higher solution concentration or a longer exposure time leads to more doping, as evidenced by successive increases in I_D going from 0.1 mM to 10 mM concentration, and from 10 min to 24 h. The average 2D sheet carrier density (n_{2D}) in MoS_2 was extracted from the characteristic curves of several pristine and functionalized devices and is shown in Figure 1d (Supporting Information Section S1). As expected, increasing the functionalization time and solution concentration resulted in increased n_{2D}. For MoS_2 functionalized with a 10 mM Me-OED solution, the average n_{2D} exceeded the degenerate limit. Notably, the MoS_2 functionalized with a 10 mM Me-OED solution for 24 h achieved an average n_{2D} of $1.10 \pm 0.37 \times 10^{14}$ cm^{-2}, the highest doping level reported to date for molecular doping to MoS_2.

To further examine the molecular doping of Me-OED to MoS_2, we performed X-ray photoelectron spectroscopy (XPS), photoluminescence (PL) measurements, and Raman spectroscopy of pristine and functionalized MoS_2 using a 10 mM Me-OED solution for 10 min (XPS data for MoS_2 functionalized using a 0.1 mM Me-OED solution for 10 min is in Figure S3). After functionalization with Me-OED, the binding energies of the Mo *3d* and S *2p* core levels decreased by 0.30 and 0.32 eV,

https://doi.org/10.1021/acs.nanolett.2c01167
Nano Lett. 2022, 22, 4501−4508

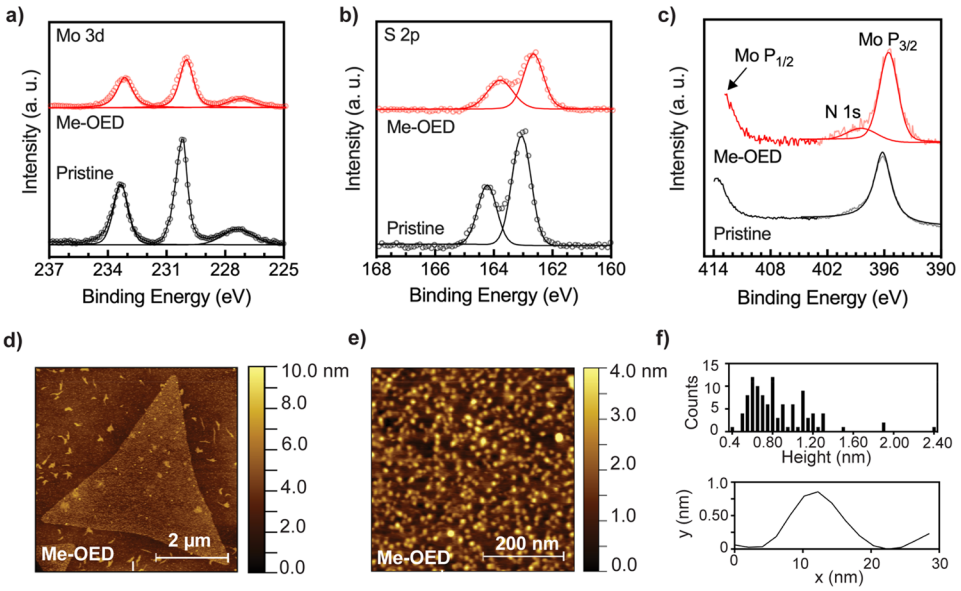

Figure 2. XPS and AFM characterization of MoS_2 functionalized with Me-OED. (a–c) XPS spectra of (a) Mo *3d*, (b) S *2p*, (c) and N *1s* core levels of pristine and functionalized MoS_2 using a 10 mM Me-OED solution for 10 min. The downward shift in binding energies for the core levels indicates the lower oxidation states of Mo and S due to electron donation to MoS_2 from the molecules. (d, e) Whole flake and zoom-in AFM images of MoS_2 functionalized with a 0.1 mM Me-OED solution for 10 min. (f) (Top) Height distributions of the molecular islands formed on MoS_2 after functionalization with a 0.1 mM Me-OED solution for 10 min. (Bottom) Example line profile of a Me-OED molecular island.

respectively (Figure 2a,b). The PL measurements show that functionalization results in quenching of the A peak of MoS_2, which also shifts to a lower energy (Figure S4). Lastly, the Raman spectrum shows that MoS_2 remains in the 2H phase and a slight red-shift in the A_{1g} band was observed after functionalization (Figure S5). Thus, XPS, PL, and Raman characterizations clearly demonstrate electron transfer from Me-OED to MoS_2, consistent with the FET measurements and previous literature studies.[6,27,28]

The XPS N *1s* peak, which is absent in pristine MoS_2, emerges after functionalization due to the presence of nitrogen atoms in Me-OED, confirming the presence of Me-OED on MoS_2 after functionalization (Figure 2c). The surface coverage of the Me-OED molecules on MoS_2 could be obtained by analyzing the ratio of the N *1s* to Mo $P_{3/2}$ peaks, which represents the ratio of dopant molecules per Mo atoms in MoS_2.[4] However, previously we showed that molecules in direct contact with MoS_2 donate electrons most strongly while molecules further away from MoS_2 only weakly donate electrons.[4] As the number of molecules obtained from XPS does not represent the percentage of molecules in close proximity to the MoS_2 surface, XPS data alone are insufficient to estimate the number of molecules that donate charge to MoS_2.

The molecular doping power is equal to the increase in MoS_2 carrier density from molecular functionalization (Δn_{2D}) divided by the number of molecules that donate charge. We previously found AFM can provide reliable estimates of the surface coverage of molecules for lower concentrations,[4] allowing for the calculation of the doping power. Surface topographic images of MoS_2 flakes functionalized with a 0.1 mM Me-OED solution for 10 min were obtained with AFM, as shown in Figure 2d and e, and the height distributions for islands are shown in Figure 2f. For the functionalized MoS_2, the surface roughness of the uncovered areas was comparable to that of pristine MoS_2 flakes (Figure S1) indicating that the uncovered areas are free of isolated molecules. The AFM images reveal that Me-OED molecules aggregate into round islands with an average diameter of 10.50 nm after deconvolving the AFM tip diameter, and there is a broad distribution of island heights (Figure 2f). The lack of clear step heights suggests that Me-OED molecules do not form discrete layers in which the aromatic ring of the molecule stacks on top of the MoS_2 surface or on top of each other. This is consistent with DFT calculations, which are discussed later.

Analysis of the AFM images reveals that the average surface coverage of Me-OED on MoS_2 is ~40% for functionalization conditions of 0.1 mM concentration of Me-OED and 10 min exposure time, and ~82% for functionalization conditions of 10 mM concentration of Me-OED and 10 min exposure time (Supporting Information Section S1; Figure S6). We note that functionalization of MoS_2 with only the solvent (acetonitrile) yields an average surface coverage of ~0.2%; thus, the islands observed are not from solvent molecules.

The doping power of Me-OED was calculated using the surface coverage estimated by AFM, following our previous study on DMAP-OED molecules (Supporting Information Section S1).[4] At functionalization conditions of a 10 mM solution for 10 min, Me-OED donates −0.22 to −0.44*e* per molecule (where *e* stands for the elementary charge), depending on whether the molecule's aromatic ring is assumed to be tilted away from or parallel with the basal plane of MoS_2 (Supporting Information Section S1). At functionalization conditions of a 0.1 mM solution for 10 min, the estimated doping power of Me-OED was very small. At such low solution concentrations, we suspect that molecules are isolated and more prone to oxidation, which would lead to degradation of the molecules and weakening of their doping ability.

We hypothesize that the compact size of Me-OED leads to high surface coverage on MoS_2 and thus maximizes doping efficiency. To confirm, we repeated our functionalization experiments using ^{t}Bu-OED, an OED with an identical redox potential as Me-OED but a larger surface area. ^{t}Bu-OED was synthesized according to a previously published procedure[29]

https://doi.org/10.1021/acs.nanolett.2c01167
Nano Lett. 2022, 22, 4501−4508

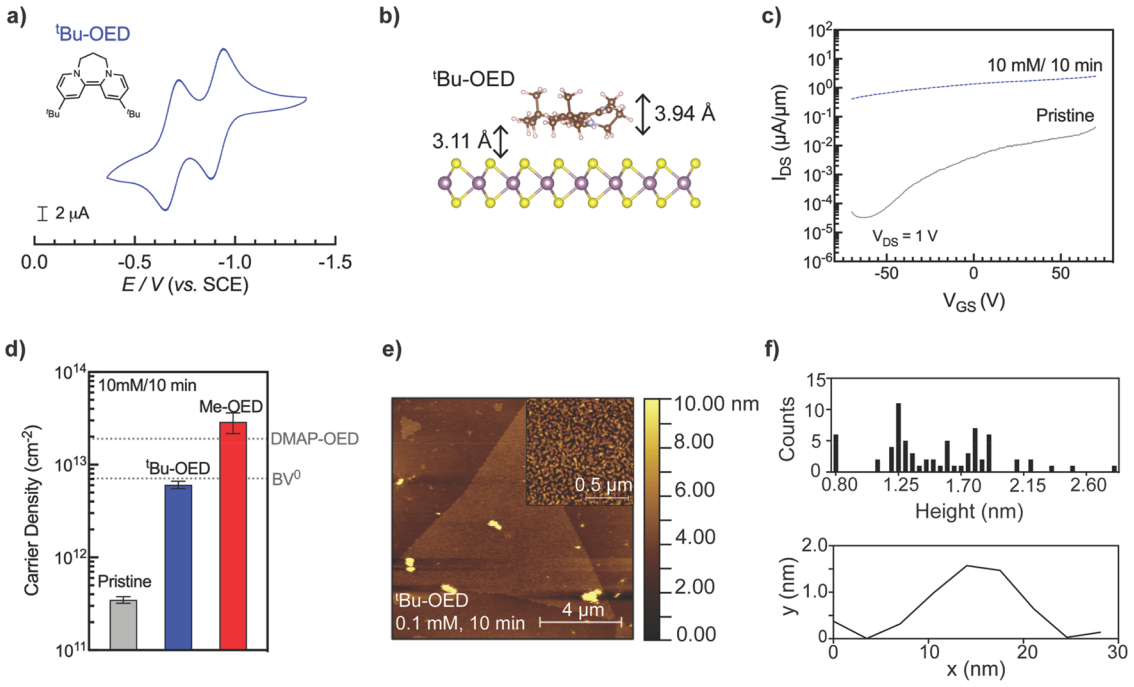

Figure 3. Cyclic voltammogram (CV) of ^{t}Bu-OED, transfer characteristics of MoS_2 FETs, and AFM characterization for MoS_2 functionalized with ^{t}Bu-OED. (a) Chemical structure and CV scan of ^{t}Bu-OED. (b) Atomic structure of a ^{t}Bu-OED molecule on MoS_2 from DFT calculations. (c) $I_{DS}-V_{GS}$ transfer curves of MoS_2 FET functionalized with a 10 mM ^{t}Bu-OED solution for 10 min, with a pristine MoS_2 FET in gray for comparison. The bias voltage is 1 V and the channel length of the devices is 3 μm. (d) Average carrier density at V_{GS} = 0 V for pristine (gray), ^{t}Bu-OED (blue), and Me-OED (red) functionalized MoS_2 FETs using a 10 mM solution and a 10 min exposure time. The error bars represent the standard error obtained from measuring 4 to 6 MoS_2 devices. (e) AFM image of MoS_2 functionalized with a 0.1 mM ^{t}Bu-OED solution for 10 min. Inset: Zoom-in image of the functionalized flake. (f) (Top) Height distributions of the molecular islands formed on MoS_2 after functionalization with a 0.1 mM ^{t}Bu-OED solution for 10 min. (Bottom) Example line profile of a ^{t}Bu-OED molecular island.

and is a neutral reductant that is stable and soluble in organic solvents under an inert atmosphere. ^{t}Bu-OED undergoes the same two discrete one-electron transfer events at −0.91 V and −0.67 V versus SCE as Me-OED, indicating they have identical redox potentials (Figure 3a). As determined by DFT calculations (Supporting Information Section S1), in isolation, the aromatic rings of ^{t}Bu-OED are nearly parallel to the basal plane of MoS_2, and ^{t}Bu-OED occupies a larger surface area than Me-OED on MoS_2 due to its larger ^{t}Bu substituents (Figure 3a,b).

The transfer characteristics of pristine and ^{t}Bu-OED functionalized MoS_2 FETs are shown in Figure 3c. After functionalization with a 10 mM ^{t}Bu-OED solution for 10 min, I_{DS} at zero V_{GS} increased by three orders of magnitude and the gate dependency of I_{DS} diminished, indicating that ^{t}Bu-OED is a strong n-type dopant. Figure 3d shows n_{2D} in MoS_2 functionalized with 10 mM solutions of Me- and ^{t}Bu-OED for 10 min. Under these conditions, Me-OED functionalization leads to greater change in the carrier density of MoS_2 than ^{t}Bu-OED functionalization. Even at the highest functionalization conditions tested (10 mM solution for 24 h), Me-OED still outperforms ^{t}Bu-OED (Figure S7). Thus, despite having the same redox potential as ^{t}Bu-OED, Me-OED is a superior dopant to MoS_2.

We also performed XPS, PL, and Raman spectroscopy for ^{t}Bu-OED functionalized MoS_2, and they show similar results to Me-OED functionalized MoS_2, confirming electron donation from ^{t}Bu-OED to MoS_2 (Figures S3, S4, S5, and S8). Figure 3e shows an AFM image of MoS_2 functionalized with a 0.1 mM ^{t}Bu-OED solution for 10 min. The AFM image reveals that ^{t}Bu-OED aggregates into islands atop MoS_2, and the islands are interconnected and chain-like. Although the height of Me-OED islands did not have clear steps, the height distribution of the ^{t}Bu-OED islands showed sharp peaks at 0.80 and 1.25 nm. This suggests formation of well-defined mono- and bilayers of ^{t}Bu-OED islands as the height of the ^{t}Bu-OED molecule is ∼0.45 nm and the distance between the molecule and MoS_2 surface is ∼0.20 nm. Analysis of the AFM images reveals that the average surface coverage was only ∼57% for ^{t}Bu-OED for functionalization conditions of 10 mM concentration and 10 min, whereas it was ∼82% for Me-OED (Figure S6). The doping power for ^{t}Bu-OED is estimated to be −0.11e per molecule, in comparison to Me-OED that donates −0.22 to 0.44e per molecule.

We performed DFT calculations investigating Me- and ^{t}Bu-OED on monolayer MoS_2 under varying surface coverages to understand the interplay between molecular structure and doping power from first principles. We first consider monolayer and submonolayer molecular coverages on MoS_2. For both OEDs, the densest coverage simulated for a monolayer of molecules with their aromatic rings parallel to the MoS_2 surface is 1/12 (one molecule per 12 formula units of MoS_2; Figure 4a for the Me-OED case). We observe that the charge donation per molecule is similar for Me- and ^{t}Bu-OED for the same molecular coverages up to 1/12 (Figure 4c), which is expected due to the identical redox potentials for the two OEDs. The charge transfer per molecule decreases as the coverage increases due to repulsive intermolecular interactions, and at a coverage of 1/12, the charge transfer per molecule is computed to be −0.36e and −0.38e per molecule for Me- and

https://doi.org/10.1021/acs.nanolett.2c01167
Nano Lett. 2022, 22, 4501−4508

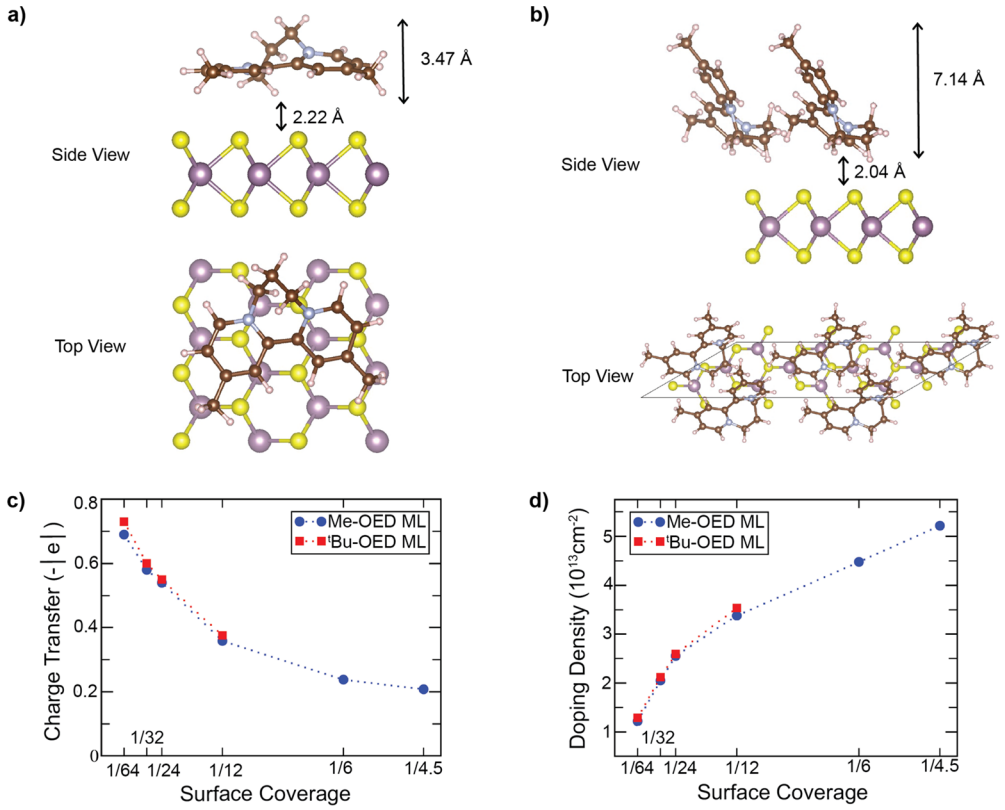

Figure 4. Molecular arrangements and doping powers as a function of surface coverage. (a, b) Monolayer arrangements of Me-OED molecules on MoS_2: side view (top panel) and top view (bottom panel) at (a) 1/12 coverage and (b) 1/6 coverage. (c) Charge transfer per molecule as a function of surface coverage. (d) Total electron doping density of monolayer OEDs on MoS_2 as predicted by DFT. The OED surface coverages are in units of one molecule per number of formula units of MoS_2 (e.g., a coverage of 1/12 refers to one molecule per 12 formula units of MoS_2). Dotted lines are guides for the eye.

^{t}Bu-OED, respectively. Higher monolayer coverages than 1/12, such as 1/6 and 1/4.5, are possible for Me-OED if the aromatic rings are tilted (Figure 4b) rather than parallel to the MoS_2 surface. In this case, the doping power per Me-OED molecule is computed to be $-0.24e$ for 1/6 coverage and $-0.21e$ for 1/4.5 coverage (Figure 4c). For ^{t}Bu-OED, our DFT calculations find that a 1/6 coverage of ^{t}Bu-OED with tilted molecules is unstable because the bulky ^{t}Bu groups are likely to hinder the formation of a densely packed monolayer.[30]

The binding energies per molecule for the bilayers of molecules are just ~0.1−0.3 eV less than those for the monolayers (Table 1). Comparing the energetics of monolayer and bilayer molecular coverages, we find that Me-OED molecules prefer to form a monolayer with tilted aromatic rings rather than a bilayer with parallel aromatic rings. These predictions are consistent with the AFM height distributions (Figures 2f and 3f), which show a broad distribution of island heights for Me-OED, in contrast to clear step heights for ^{t}Bu-OED, corresponding to mono- and bilayers of ^{t}Bu-OED molecules. As such, we attribute the impressive doping power of Me-OED to its compact size, which allows it to pack more efficiently with tilted aromatic rings.

Table 1. DFT-Calculated Binding Energies Per Molecule for Monolayer and Bilayer OED Molecules on MoS_2

binding energy (eV)	Me-OED @ 1/12 surface coverage	Me-OED @ 1/6 surface coverage	^{t}Bu-OED @ 1/12 surface coverage
monolayer	1.74	1.79	2.07
bilayer (on top of MoS_2)	1.44	1.63	1.88
bilayer (molecule on top rotated by 90 deg)	1.52	-	1.89

The calculated doping powers of densely covered Me-OED ($-0.21e$ to $-0.36e$ per molecule at 1/4.5 and 1/6 surface coverage) agree well with the experimental values ($-0.22e$ to $-0.44e$). However, for ^{t}Bu-OED, the calculated doping power per molecule ($-0.38e$) is much larger than the experimental value ($-0.11e$) estimated for functionalization conditions of 10 mM solution for 10 min. However, a densely packed molecular arrangement might not be reached for ^{t}Bu-OED after an exposure time of 10 min because the surface kinetics of ^{t}Bu-OED on MoS_2 are slow. This reasoning is based on our observation that the surface coverage and average n_{2D} for MoS_2 functionalized with a 10 mM solution of ^{t}Bu-OED for 1 and 10 min are identical (Figure S9). In our calculations, we assume that the ^{t}Bu-OED islands observed by AFM take the molecular arrangement of the densely packed 1/12 surface coverage. Yet, there may be fewer ^{t}Bu-OED molecules per unit area in the observed molecular islands than what we estimate. For MoS_2 functionalized with a 10 mM ^{t}Bu-OED solution for 24 h, the average surface coverage is ~51% (Figure S10) and the estimated doping power of ^{t}Bu-OED is approximately $-0.46e$, in good agreement with DFT calculations ($-0.38e$).

Having calculated the molecular doping powers of Me- and ^{t}Bu-OED to MoS_2 at varying surface coverages, we also computed the average n_{2D} of functionalized MoS_2 to compare

https://doi.org/10.1021/acs.nanolett.2c01167
Nano Lett. 2022, 22, 4501−4508

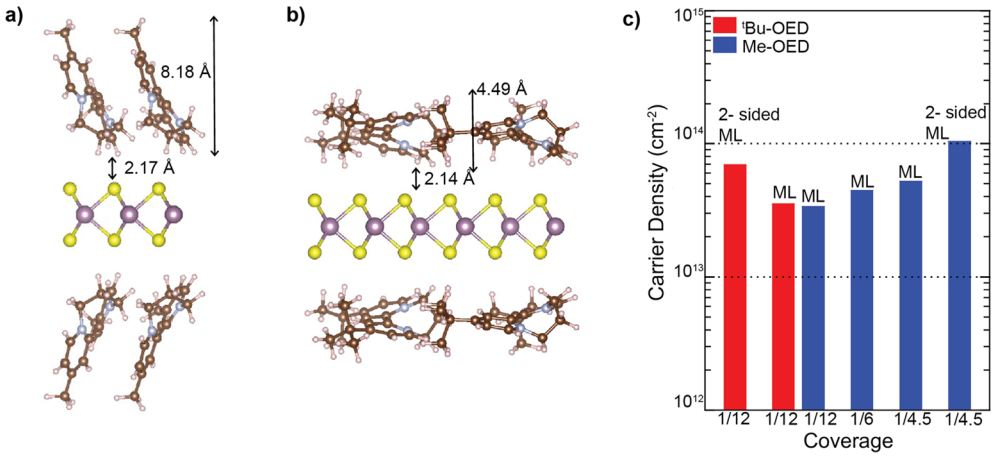

Figure 5. Double surface-functionalization with OEDs. (a) Side view of monolayers of Me-OED with tilted rings covering both sides of MoS_2 at 1/4.5 surface coverage (i.e., two molecules cover a 3 × 3 supercell of MoS_2). (b) Side view of monolayers of ^{t}Bu-OED covering both sides of MoS_2 at 1/12 surface coverage. (c) Summary of DFT-calculated total electron doping densities for both OEDs at the denser coverage regimes for monolayer coverage on a top surface of MoS_2 (labeled "ML") or both surfaces of MoS_2 (labeled "2-sided ML").

with the experimentally determined n_{2D}. The computed n_{2D} is 5.2×10^{13} cm^{-2} for Me-OED at 1/4.5 coverage and 3.5×10^{13} cm^{-2} for ^{t}Bu-OED at 1/12 coverage (Figure 4d), which are in the same order of magnitude as the experimental values (Figures 1d and 3d). However, for the maximum functionalization conditions (10 mM solution, 24 h), the computed n_{2D} is almost half the experimental n_{2D}. With a settling time of 24 h, we hypothesize that OED molecules might intercalate between the MoS_2 and the substrate, functionalizing both surfaces of the MoS_2 monolayer.[31] We simulate this scenario for a 1/4.5 surface coverage of Me-OED and a 1/12 surface coverage of ^{t}Bu-OED (the densest monolayer coverage). Figure 5a and b show the corresponding relaxed geometries for the Me- and ^{t}Bu-OED cases, respectively. We find that adsorption on both sides of MoS_2, instead of one side, does not change the binding energies per molecule significantly, while the corresponding electron doping density is approximately doubled. As a result, the highest n_{2D} values computed are 1.04×10^{14} cm^{-2} for Me-OED functionalized MoS_2 and 7.0×10^{13} cm^{-2} for ^{t}Bu-OED functionalized MoS_2 (Figure 5c). These numbers are in good agreement with the experimental results ($1.10 \pm 0.37 \times 10^{14}$ cm^{-2} for Me-OED and $4.83 \pm 0.90 \times 10^{13}$ cm^{-2} for ^{t}Bu-OED for the optimal functionalization conditions; Figure 1d; Figure S9).

Our results demonstrate that despite having the same redox potential, the doping powers of Me- and ^{t}Bu-OED vary due to differences in their size. This affects their interactions with MoS_2, which is reflected in the distinct morphologies and height distributions of the Me- and ^{t}Bu-OED islands. Further, molecular size impacts the molecular packing efficiency, an important parameter for the total charge donation to MoS_2. The stronger doping power of Me-OED compared to ^{t}Bu-OED is attributed to the smaller size of Me-OED, which allows for better packing efficiency, thus maximizing the total charge transferred from the molecules to MoS_2. DFT calculations of the molecular doping power and achievable carrier density agree well with the experimental results and demonstrate that the highest carrier density observed can be achieved via double-surface functionalization. Thus, optimal molecular dopants should possess a maximally negative redox potential, be small, and achieve a high packing efficiency with the 2D surface.

■ ASSOCIATED CONTENT

Supporting Information

The Supporting Information is available free of charge at https://pubs.acs.org/doi/10.1021/acs.nanolett.2c01167.

Additional experimental details, surface characterizations (AFM, XPS, PL, and Raman), average carrier densities for functionalized MoS_2, NMR spectra for organic reductant molecules (PDF)

■ AUTHOR INFORMATION

Corresponding Author

Judy J. Cha − *Department of Mechanical Engineering and Materials Science, Yale University, New Haven, Connecticut 06511, United States; Energy Sciences Institute, Yale West Campus, West Haven, Connecticut 06516, United States;* orcid.org/0000-0002-6346-2814; Email: judy.cha@yale.edu

Authors

Serrae N. Reed-Lingenfelter − *Department of Mechanical Engineering and Materials Science, Yale University, New Haven, Connecticut 06511, United States; Energy Sciences Institute, Yale West Campus, West Haven, Connecticut 06516, United States;* orcid.org/0000-0003-0112-7030

Yifeng Chen − *Department of Physics, National University of Singapore, 117551, Singapore;* orcid.org/0000-0003-4216-8242

Milad Yarali − *Department of Mechanical Engineering and Materials Science, Yale University, New Haven, Connecticut 06511, United States; Energy Sciences Institute, Yale West Campus, West Haven, Connecticut 06516, United States*

David J. Charboneau − *Department of Chemistry, Yale University, New Haven, Connecticut 06511, United States*

Julia B. Curley − *Department of Chemistry, Yale University, New Haven, Connecticut 06511, United States*

David J. Hynek − *Department of Mechanical Engineering and Materials Science, Yale University, New Haven, Connecticut 06511, United States; Energy Sciences Institute, Yale West Campus, West Haven, Connecticut 06516, United States*

Mengjing Wang − *Department of Mechanical Engineering and Materials Science, Yale University, New Haven, Connecticut 06511, United States; Energy Sciences Institute, Yale West*

https://doi.org/10.1021/acs.nanolett.2c01167
Nano Lett. 2022, 22, 4501−4508

Campus, West Haven, Connecticut 06516, United States; orcid.org/0000-0003-1195-4515

Natalie L. Williams − *Energy Sciences Institute, Yale West Campus, West Haven, Connecticut 06516, United States; Department of Chemistry, Yale University, New Haven, Connecticut 06511, United States*

Nilay Hazari − *Department of Chemistry, Yale University, New Haven, Connecticut 06511, United States;* orcid.org/0000-0001-8337-198X

Su Ying Quek − *Department of Physics, National University of Singapore, 117551, Singapore; Centre for Advanced 2D Materials, National University of Singapore, 117546, Singapore;* orcid.org/0000-0003-4223-2953

Complete contact information is available at: https://pubs.acs.org/10.1021/acs.nanolett.2c01167

Notes

The authors declare no competing financial interest.

■ ACKNOWLEDGMENTS

The synthesis of MoS_2 flakes was supported by a CAREER award from the NSF (1749742) and device measurements after surface functionalization were supported by the Army Research Office (W911NF-18-1-0367). S.N.R.-L. acknowledges the Ford Foundation for a graduate student fellowship, while J.B.C. thanks the NSF for a graduate research fellowship. We thank Dr. Fabian Menges for assistance with high-resolution mass spectrometry. Material characterizations were carried out at shared facilities including the Yale West Campus Materials Characterization Core, the Yale Institute for Nanoscience and Quantum Engineering, and the School of Engineering Cleanroom. S.Y.Q. and Y.C. acknowledge funding from the Grant MOE2016-T2-2-132 from the Ministry of Education, Singapore, and support from the Singapore National Research Foundation, Prime Minister's Office, under its medium-sized centre program. Computations were performed on the NUS Graphene Research Centre cluster and National Supercomputing Centre Singapore.

■ REFERENCES

(1) Zhao, Y.; Gobbi, M.; Hueso, L.; Samorì, P. Molecular Approach to Engineer Two-Dimensional Devices for CMOS and beyond-CMOS Applications. *ACS Chemical Reviews* **2022**, *122* (1), 50−131.

(2) Bhimanapati, G. R.; Lin, Z.; Meunier, V.; Jung, Y.; Cha, J.; Das, S.; Xiao, D.; Son, Y.; Strano, M. S.; Cooper, V. R.; Liang, L.; Louie, S. G.; Ringe, E.; Zhou, W.; Kim, S. S.; Naik, R. R.; Sumpter, B. G.; Terrones, H.; Xia, F.; Wang, Y.; Zhu, J.; Akinwande, D.; Alem, N.; Schuller, J. A.; Schaak, R. E.; Terrones, M.; Robinson, J. A. Recent Advances in Two-Dimensional Materials beyond Graphene. *ACS Nano* **2015**, *9* (12), 11509−11539.

(3) Gobbi, M.; Orgiu, E.; Samorì, P. When 2D Materials Meet Molecules: Opportunities and Challenges of Hybrid Organic/Inorganic van der Waals Heterostructures. *Adv. Mater.* **2018**, *30* (18), 1706103.

(4) Yarali, M.; Zhong, Y.; Reed, S. N.; Wang, J.; Ulman, K. A.; Charboneau, D. J.; Curley, J. B.; Hynek, D. J.; Pondick, J. V.; Yazdani, S.; Hazari, N.; Quek, S. Y.; Wang, H.; Cha, J. J. Near-Unity Molecular Doping Efficiency in Monolayer MoS2. *Advanced Electronic Materials* **2021**, *7* (2), 2000873.

(5) Wehling, T. O.; Novoselov, K. S.; Morozov, S. V.; Vdovin, E. E.; Katsnelson, M. I.; Geim, A. K.; Lichtenstein, A. I. Molecular Doping of Graphene. *Nano Lett.* **2008**, *8* (1), 173−177.

(6) Bertolazzi, S.; Gobbi, M.; Zhao, Y.; Backes, C.; Samorì, P. Molecular chemistry approaches for tuning the properties of two-dimensional transition metal dichalcogenides. *Chem. Soc. Rev.* **2018**, *47* (17), 6845−6888.

(7) Schedin, F.; Geim, A. K.; Morozov, S. V.; Hill, E. W.; Blake, P.; Katsnelson, M. I.; Novoselov, K. S. Detection of individual gas molecules adsorbed on graphene. *Nat. Mater.* **2007**, *6* (9), 652−655.

(8) Kiriya, D.; Tosun, M.; Zhao, P.; Kang, J. S.; Javey, A. Air-Stable Surface Charge Transfer Doping of MoS2 by Benzyl Viologen. *J. Am. Chem. Soc.* **2014**, *136* (22), 7853−7856.

(9) Yu, W. J.; Liao, L.; Chae, S. H.; Lee, Y. H.; Duan, X. Toward tunable band gap and tunable dirac point in bilayer graphene with molecular doping. *Nano Lett.* **2011**, *11* (11), 4759−4763.

(10) Wei, P.; Liu, N.; Lee, H. R.; Adijanto, E.; Ci, L.; Naab, B. D.; Zhong, J. Q.; Park, J.; Chen, W.; Cui, Y.; Bao, Z. Tuning the Dirac Point in CVD-Grown Graphene through Solution Processed n-Type Doping with 2-(2-Methoxyphenyl)-1,3-dimethyl-2,3-dihydro-1H-benzoimidazole. *Nano Lett.* **2013**, *13* (5), 1890−1897.

(11) Park, J.; Jo, S. B.; Yu, Y.-J.; Kim, Y.; Yang, J. W.; Lee, W. H.; Kim, H. H.; Hong, B. H.; Kim, P.; Cho, K.; Kim, K. S. Single-Gate Bandgap Opening of Bilayer Graphene by Dual Molecular Doping. *Adv. Mater.* **2012**, *24* (3), 407−411.

(12) Zhu, X.; Guo, Y.; Cheng, H.; Dai, J.; An, X.; Zhao, J.; Tian, K.; Wei, S.; Cheng Zeng, X.; Wu, C.; Xie, Y. Signature of coexistence of superconductivity and ferromagnetism in two-dimensional NbSe2 triggered by surface molecular adsorption. *Nat. Commun.* **2016**, *7* (1), 11210.

(13) Samuels, A. J.; Carey, J. D. Molecular Doping and Band-Gap Opening of Bilayer Graphene. *ACS Nano* **2013**, *7* (3), 2790−2799.

(14) Yoshizawa, S.; Minamitani, E.; Vijayaraghavan, S.; Mishra, P.; Takagi, Y.; Yokoyama, T.; Oba, H.; Nitta, J.; Sakamoto, K.; Watanabe, S.; Nakayama, T.; Uchihashi, T. Controlled Modification of Superconductivity in Epitaxial Atomic Layer−Organic Molecule Heterostructures. *Nano Lett.* **2017**, *17* (4), 2287−2293.

(15) Cho, K.; Pak, J.; Kim, J.-K.; Kang, K.; Kim, T.-Y.; Shin, J.; Choi, B. Y.; Chung, S.; Lee, T. Contact-Engineered Electrical Properties of MoS2 Field-Effect Transistors via Selectively Deposited Thiol-Molecules. *Adv. Mater.* **2018**, *30* (18), 1705540.

(16) de Boer, B.; Hadipour, A.; Mandoc, M. M.; van Woudenbergh, T.; Blom, P. W. M. Tuning of Metal Work Functions with Self-Assembled Monolayers. *Adv. Mater.* **2005**, *17* (5), 621−625.

(17) Huang, Y. L.; Zheng, Y. J.; Song, Z.; Chi, D.; Wee, A. T. S.; Quek, S. Y. The organic−2D transition metal dichalcogenide heterointerface. *Chem. Soc. Rev.* **2018**, *47* (9), 3241−3264.

(18) Lee, S. Y.; Duong, D. L.; Vu, Q. A.; Jin, Y.; Kim, P.; Lee, Y. H. Chemically Modulated Band Gap in Bilayer Graphene Memory Transistors with High On/Off Ratio. *ACS Nano* **2015**, *9* (9), 9034−9042.

(19) Mouri, S.; Miyauchi, Y.; Matsuda, K. Tunable Photoluminescence of Monolayer MoS2 via Chemical Doping. *Nano Lett.* **2013**, *13* (12), 5944−5948.

(20) Pak, J.; Jang, J.; Cho, K.; Kim, T.-Y.; Kim, J.-K.; Song, Y.; Hong, W.-K.; Min, M.; Lee, H.; Lee, T. Enhancement of photodetection characteristics of MoS2 field effect transistors using surface treatment with copper phthalocyanine. *Nanoscale* **2015**, *7* (44), 18780−18788.

(21) Stoeckel, M.-A.; Gobbi, M.; Leydecker, T.; Wang, Y.; Eredia, M.; Bonacchi, S.; Verucchi, R.; Timpel, M.; Nardi, M. V.; Orgiu, E.; Samorì, P. Boosting and Balancing Electron and Hole Mobility in Single- and Bilayer WSe2 Devices via Tailored Molecular Functionalization. *ACS Nano* **2019**, *13* (10), 11613−11622.

(22) Tarasov, A.; Zhang, S.; Tsai, M.-Y.; Campbell, P. M.; Graham, S.; Barlow, S.; Marder, S. R.; Vogel, E. M. Controlled Doping of Large-Area Trilayer MoS2 with Molecular Reductants and Oxidants. *Adv. Mater.* **2015**, *27* (7), 1175−1181.

(23) Zhang, S.; Hill, H. M.; Moudgil, K.; Richter, C. A.; Hight Walker, A. R.; Barlow, S.; Marder, S. R.; Hacker, C. A.; Pookpanratana, S. J. Controllable, Wide-Ranging n-Doping and p-Doping of Monolayer Group 6 Transition-Metal Disulfides and Diselenides. *Adv. Mater.* **2018**, *30* (36), 1802991.

(24) Cho, K.; Pak, J.; Chung, S.; Lee, T. Recent Advances in Interface Engineering of Transition-Metal Dichalcogenides with

Organic Molecules and Polymers. *ACS Nano* **2019**, *13* (9), 9713−9734.
(25) Kim, J.-K.; Cho, K.; Jang, J.; Baek, K.-Y.; Kim, J.; Seo, J.; Song, M.; Shin, J.; Kim, J.; Parkin, S. S. P.; Lee, J.-H.; Kang, K.; Lee, T. Molecular Dopant-Dependent Charge Transport in Surface-Charge-Transfer-Doped Tungsten Diselenide Field Effect Transistors. *Adv. Mater.* **2021**, *33* (44), 2101598.
(26) Song, Z.; Wang, Q.; Li, M.-Y.; Li, L.-J.; Zheng, Y. J.; Wang, Z.; Lin, T.; Chi, D.; Ding, Z.; Huang, Y. L.; Thye Shen Wee, A. Liquid-solid surface phase transformation of fluorinated fullerene on monolayer tungsten diselenide. *Phys. Rev. B* **2018**, *97* (13), 134102.
(27) Wang, H.; Lu, Z.; Xu, S.; Kong, D.; Cha, J. J.; Zheng, G.; Hsu, P.-C.; Yan, K.; Bradshaw, D.; Prinz, F. B.; Cui, Y. Electrochemical tuning of vertically aligned MoS2 nanofilms and its application in improving hydrogen evolution reaction. *Proc. Natl. Acad. Sci. U. S. A.* **2013**, *110* (49), 19701.
(28) Wang, Y.; Slassi, A.; Stoeckel, M.-A.; Bertolazzi, S.; Cornil, J.; Beljonne, D.; Samorì, P. Doping of Monolayer Transition-Metal Dichalcogenides via Physisorption of Aromatic Solvent Molecules. *J. Phys. Chem. Lett.* **2019**, *10* (3), 540−547.
(29) Rueping, M.; Nikolaienko, P.; Lebedev, Y.; Adams, A. Metal-free reduction of the greenhouse gas sulfur hexafluoride, formation of SF5 containing ion pairs and the application in fluorinations. *Green Chem.* **2017**, *19* (11), 2571−2575.
(30) Ulman, A. Formation and Structure of Self-Assembled Monolayers. *Chem. Rev.* **1996**, *96* (4), 1533−1554.
(31) Kim, H. H.; Yang, J. W.; Jo, S. B.; Kang, B.; Lee, S. K.; Bong, H.; Lee, G.; Kim, K. S.; Cho, K. Substrate-Induced Solvent Intercalation for Stable Graphene Doping. *ACS Nano* **2013**, *7* (2), 1155−1162.

https://doi.org/10.1021/acs.nanolett.2c01167
Nano Lett. 2022, 22, 4501−4508